Phase Transition in Perovskite Oxide $La_{0.75}Sr_{0.25}Cr_{0.5}Mn_{0.5}O_{3-\delta}$ Observed by in Situ High-Temperature Neutron Powder Diffraction

Shanwen Tao and John T. S. Irvine*

School of Chemistry, University of St Andrews, Fife KY16 9ST, Scotland, UK

Received June 17, 2006. Revised Manuscript Received August 25, 2006

$(La_{0.75}Sr_{0.25})Cr_{0.5}Mn_{0.5}O_{3-\delta}$ (LSCM) has recently been shown to be an efficient redox stable anode for solid oxide fuel cells (SOFCs). The structure of LSCM has been investigated by X-ray diffraction and neutron diffraction to further understand its properties under SOFC operating conditions. Samples were prepared with nominal A-site deficiency; however, neutron diffraction demonstrates that the A-site deficiency is actually minimal or even null, with spinel impurity compensating for low content of A-site species. This was not apparent from XRD. The perovskite oxide $La_{0.75}Sr_{0.25}Cr_{0.5}Mn_{0.5}O_3$ (LSCM) exhibits a rhombohedral structure with space group $R\bar{3}c$ (167), $a = 5.4479(1)$ Å, $\beta = 60.477(1)°$, and $V = 115.563$ Å^3 at room temperature. Conductivity and thermal expansion data in air exhibit an anomalous change starting at ~400 °C which we here demonstrate as being correlated to a phase transition. The perovskite phase undergoes a $R\bar{3}c \rightarrow Pm\bar{3}m$, rhombohedral to cubic phase transition over the temperature range from 500 to over 1100 °C as observed using in situ high-temperature neutron powder diffraction. The fraction of the cubic phase increases with increasing temperature and reaches 85% at 1000 °C. The phase transition is gradual; therefore, any sudden volume change due to a phase transition would be minimized, allowing a good electrolyte/anode interface on thermal cycling. The reduced form of $La_{0.75}Sr_{0.25}Cr_{0.5}Mn_{0.5}O_{3-\delta}$ exhibits a primitive cubic structure with space group $Pm\bar{3}m$, which is the same as the major phase of $La_{0.75}Sr_{0.25}Cr_{0.5}Mn_{0.5}O_3$ in air at high temperatures; therefore, the stresses due to phase changes on redox cycling may be minimized.

1. Introduction

Perovskite oxides are a very important class of materials due to their application as catalysts,[1] magnetic, and electric materials.[2,3] Perovskite oxides have been widely investigated as electrolyte and electrode materials for solid oxide fuel cells (SOFCs).[4−7] Recently, we found that the perovskite oxide $(La_{0.75}Sr_{0.25})Cr_{0.5}Mn_{0.5}O_{3-\delta}$ (LSCM) is an efficient, redox-stable anode material for SOFCs.[8−12] It was found that LSCM exhibits rhombohedral structure at room temperature from XRD analysis. After LSCM is reduced in 5% H_2/Ar at 900 °C for 120 h, it exhibits a cubic structure.[10]

Lower electrode interfacial resistance and overpotential losses have been reported when using an A-site deficient perovskite, $(La_{0.85}Sr_{0.15})_{0.9}MnO_3$, as the cathode for solid oxide fuel cells compared to the stoichiometric $(La_{0.85}Sr_{0.15})_{1.0}MnO_3$.[13] The much poorer performance of the latter is believed to be due to the formation of resistive substances such as $La_2Zr_2O_7/SrZrO_3$ between LSM and YSZ phases in the composite electrode and at the electrode/electrolyte interface.[13,14] A-site deficiency is also often used to extend the stability range in perovskites by decreasing the sintering temperature and so enabling co-sintering.[15] In our experiments, a perovskite with nominal composition $(La_{0.75}Sr_{0.25})_{0.95}Cr_{0.5}Mn_{0.5}O_3$ was selected as the A-site deficiency to enhance stability against interfacial reaction.

The structure of perovskite can be very complicated due to the tilting of the octahedra and the ordering of both A- and B-site elements.[16−21] Perovskite oxides may undergo several phase transitions at high temperatures as has been observed in $BaCeO_3$,[22] $Pr_{1-x}Sr_xMnO_3$,[23] and Sr_2MWO_6 (M

* Corresponding author. Tel.: +44 1334 463817. Fax: +44 1334 463808. E-mail: jtsi@st-and.ac.uk.

(1) Pena, M. A.; Fierro, J. L. G. *Chem. Rev.* **2001**, *101*, 1981.
(2) Kobayashi, K. L.; Kimura, T.; Sawada, H.; Terakura, K.; Tokura, Y. *Nature* **1998**, *395*, 677.
(3) DeMarco, M.; Blackstead, H. A.; Dow, J. D.; Wu, M. K.; Chen, D. Y.; Chien, F. Z.; Haka, M.; Toorongian, S.; Fridmann, J. *Phys. Rev. B* **2000**, *62*, 14301.
(4) Ishihara, T.; Matsuda, H.; Takita, Y. *J. Am. Chem. Soc.* **1994**, *116*, 3801.
(5) Minh, N. Q. *J. Am. Ceram. Soc.* **1993**, *76*, 563.
(6) Tao, S. W.; Irvine, J. T. S. *Chem. Rec.* **2004**, *4*, 83.
(7) Atkinson, A.; Barnett, S.; Gorte, R. J.; Irvine, J. T. S.; McEvoy, A. J.; Mogensen, M.; Singhal, S. C.; Vohs, J. *Nat. Mater.* **2004**, *3*, 17.
(8) Tao, S. W.; Irvine, J. T. S. *Nat. Mater.* **2003**, *2*, 320.
(9) Boukamp, B. A. *Nat. Mater.* **2003**, *2*, 294.
(10) Tao, S. W.; Irvine, J. T. S. *J. Electrochem. Soc.* **2004**, *151*, A252.
(11) Tao, S. W.; Irvine, J. T. S.; Kilner, J. A. *Adv. Mater.* **2005**, *17*, 1734.
(12) Zha, S. W.; Tsang, P.; Cheng, Z.; Liu, M. L. *J. Solid State Chem.* **2005**, *178*, 1844.
(13) Mitterdorfer, A.; Gauckler, L. J. *Solid State Ionics* **1998**, *111*, 185.
(14) Leng, Y. J.; Chan, S. H.; Khor, K. A.; Jiang, S. P. *J. Appl. Electrochem.* **2004**, *34*, 409.
(15) Jones, F. G. E.; Connor, P. A.; Irvine, J. T. S. *Proceedings of the 9th International Symposium on Solid Oxide Fuel Cells*; Singal, S. C., Mizusaki, J., Eds.; The Electrochemical Society Inc/: Pennington, NJ, 2005; Vol. 2, pp 1571−1576.
(16) Glazer, A. M. *Acta Crystallogr., B* **1972**, *28*, 3384.
(17) Thomas, N. W.; Bettollahi A. *Acta Crystallogr., B* **1994**, *50*, 549.
(18) Woodward, P. M. *Acta Crystallogr., B* **1997**, *53*, 32.
(19) Howard C. J.; Stokes, H. T. *Acta Crystallogr., B* **1998**, *54*, 782.
(20) Tao, S. W.; Canales-Vazquez, J.; Irvine, J. T. S. *Chem. Mater.* **2004**, *11*, 2309.
(21) Garcia-Martin, S.; Alario-Franco, M. A.; Ehrenberg, H.; Rodriguez-Carvajal, J.; Amador, U. *J. Am. Chem. Soc.* **2004**, *126*, 3587.
(22) Knight, K. S. *Solid State Ionics* **1994**, *74*, 109.
(23) Knizek, K.; Hejtmanek, J.; Jirak, Z.; Martin, C.; Hervieu, M.; Raveau, B.; André, G.; Bouree, F. *Chem. Mater.* **2004**, *16*, 1104.

10.1021/cm061413n CCC: $33.50
Published on Web 10/13/2006

= Ni, Zn, Co, Cu)[24] etc. Both first- and second-order phase transitions may occur in perovskite. Knowledge of the possible phase transitions in LSCM at elevated temperature is very important to allow a good electrolyte/anode interface to be achieved when fabricating and operating the cell at high temperature. A first-order phase transition with an abrupt volume change that might cause delamination of the electrolyte/anode interface would not be welcome. To investigate structure and phase evolution of LSCM at high temperature, an in situ neutron diffraction study has been carried out up to 1000 °C. The results of this study are presented here.

2. Experimental Section

The perovskite oxide with nominal composition $(La_{0.75}Sr_{0.25})_{0.95}Cr_{0.5}Mn_{0.5}O_3$ was synthesized using a solid-state method. To ensure good crystallinity, dried La_2O_3, $SrCO_3$, Cr_2O_3, and Mn_2O_3 powders were ground under acetone. The sample was calcined at 1100 °C for 2 h and then fired at 1400 °C for 116 h in total with intermediate grindings. The final cooling rate was 5 °C/min.

XRD analysis of powders reacted at different temperatures were carried out on a Stoe Stadi-P diffractometer to determine phase purity and measure crystal parameters. Structure refinement was performed using the Rietveld method using the program General Structure Analysis System (GSAS).[25]

The dilatometry investigation of LSCM was carried out on a NETZSCH DIL 402C dilatometer (alumina holder) with a TASC 414/4 controller. A $(La_{0.75}Sr_{0.25})_{0.95}Cr_{0.5}Mn_{0.5}O_3$ cylinder ($L \approx 30$ mm, $\phi \approx 12$ mm) with a relative density of about 95% was tested in air in the temperature range from room temperature to 950 °C at a rate of 3 °C/min.

The dc conductivity was measured by the conventional four-terminal method using a Keithley 220 Programmable Current Source and a Schlumberger Solartron 7150 Digital Multimeter for voltage measurements.

The in situ time-of-flight neutron diffraction data were collected on the POLARIS diffractometer at ISIS, the UK pulsed spallation neutron source. Diffraction patterns collected on the POLARIS backscattering detector bank were used in all data analyses. The backscattering detector bank is made up of an array of 58 ^{3}He tubes, covering an angular range of 130−160° in 2θ, thus giving access to a d-spacing range of 0.2−3.2 Å in the 20 ms time interval between successive neutron pulses from the ISIS target. The sample was put into a vanadium sample holder to minimize the diffraction from the sample container. The sample holder was put in a vacuum of 10^{-5}−10^{-4}atm during the measurements to prevent oxidation of the vanadium container.[26] The neutron diffraction data were processed and manipulated using the program Genie,[27] which enabled output of data in a format appropriate for the Rietveld refinement using the program GSAS.[25]

For the backscattering bank on POLARIS, the detectors have L ranging from 0.65 to 1.35 m. Normalization and conversion of time-of-flight to d spacing is performed within the program Genie.[26]

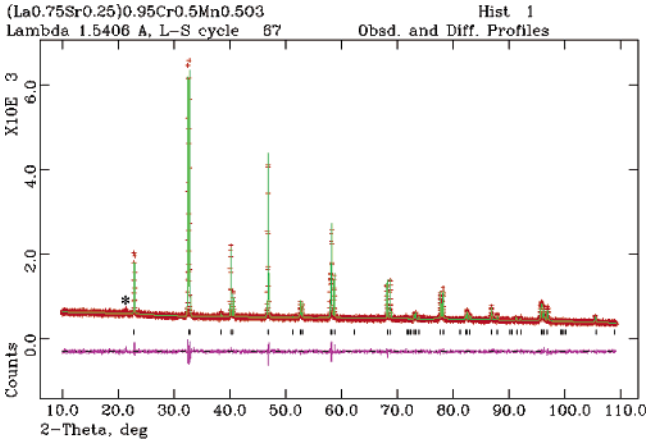

Figure 1. X-ray powder diffraction pattern of $La_{0.75}Sr_{0.25}Cr_{0.5}Mn_{0.5}O_3$ prepared at 1400 °C. * Vaseline.

The measurement was performed starting at room temperature, then increased to 200 °C, and held isothermally for an hour. Data between 200 and 1000 °C were then collected at 100 °C intervals, holding at each temperature for 1 h to reach equilibrium before data collection.

To examine any effects that the vacuum may have had on the composition of LSCM when undergoing neutron diffraction, some LSCM powders were heated under vacuum (partial pressure $\sim 10^{-5}$) in a TORVAC high-temperature furnace at 1000 °C for 10 h after these neutron experiments.

3. Results and Discussion

3.1. Structure at Room Temperature. To achieve phase purity as observed by XRD, the sample had to be fired at 1400 °C for 116 h with intermediate grindings. The X-ray diffraction pattern of an as-prepared sample with nominal composition $(La_{0.75}Sr_{0.25})_{0.95}Cr_{0.5}Mn_{0.5}O_3$ is shown in Figure 1. The material exhibits a rhombohedral structure with $a = \sqrt{2}a_p$ and $\beta \approx 60°$ from XRD data where a_p is the lattice parameter of a primitive cubic perovskite. The unit cell was refined as rhombohedral with space group $R\bar{3}c(167)$, $a = 5.4570(1)$ Å, $\beta = 60.4887(1)°$, and $V = 116.173$ Å.^{3} During the refinement, it was found that a smaller R-value was achieved when the occupancy of La and Sr was fixed to 0.75 and 0.25, respectively, rather than 0.7125 and 0.2375 as expected from the nominal formula, indicating the real composition of "$(La_{0.75}Sr_{0.25})_{0.95}Cr_{0.5}Mn_{0.5}O_{3-\delta}$" might not be A-site deficient perovskite, as also demonstrated later by neutron diffraction. Despite the apparent absence of A-site deficiency, the material appears to be pure by XRD analysis, although due to a fluorescence problem, XRD with copper radiation is not best applied to manganese-containing phases. The refined structural parameters from XRD are listed in Table 1.

Neutron diffraction was utilized to further investigate the structure. The room-temperature neutron diffraction pattern is shown in Figure 2a. The same space group, $R\bar{3}c(167)$ was applied and a good fit was achieved. During the refinement, it was found that the occupancy of La and Sr is close to 0.75 and 0.25, respectively, and that a small amount of spinel impurity was present, indicating that the real composition of "$(La_{0.75}Sr_{0.25})_{0.95}Cr_{0.5}Mn_{0.5}O_{3-\delta}$" is not actually A-site deficient. Also the oxygen occupancy refined to 1, indicating

(24) Gateshki, M.; Igartua, J. M.; Hernandez-Bocanegra, E. *J. Phys. −Condens. Matter* **2003**, *15*, 6199.
(25) Larson, A. C.; Von Dreele, R. B. GSAS-Generalised Crystal Structure Analysis Systeml Los Alamos National Laboratory Report No. LA-UR-86-748; Los Alamos National Laboratory: Los Alamos, NM, 1994.
(26) Walton, R. I.; Millange, F; Smith, R. I.; Hansen, T. C.; O'Hare, D. *J. Am. Chem. Soc.* **2001**, *123*, 12547.
(27) David, W. I. F.; Johnson, M. W.; Knowles, K. J.; Smith, C. M. M.; Crosbie, G. D.; Campbell, E. P.; Graham, S. P.; Lyall, J. S. Rutherford Appleton Laboratory Report RAL-86-102; Rutherford Appleton Laboratory: Chilton, Didcot, Oxfordshire, U.K., 1986.

Table 1. Structure Parameters of $La_{0.75}Sr_{0.25}Cr_{0.5}Mn_{0.5}O_3$ Prepared at 1400 °C Obtained from X-ray Powder Diffraction Data[a]

atom	site	occupancy	x	y	z	U_{iso} (Å^2)
La	2a	0.75	0.25	0.25	0.25	0.0123(3)
Sr	2a	0.25	0.25	0.25	0.25	0.0123(3)
Cr	2b	0.5	0	0	0	0.0130(6)
Mn	2b	0.5	0	0	0	0.0130(6)
O	6e	1	0.7928(12)	0.7071(12)	0.25	0.0108(15)

[a] Space group $R\bar{3}c$ (167); a = 5.4570(1) Å, α = 60.488(3)°, V = 116.173(1) Å^3, Z = 2. R_{wp} = 4.53%, R_p = 3.55%, χ_{red}^2 = 1.097.

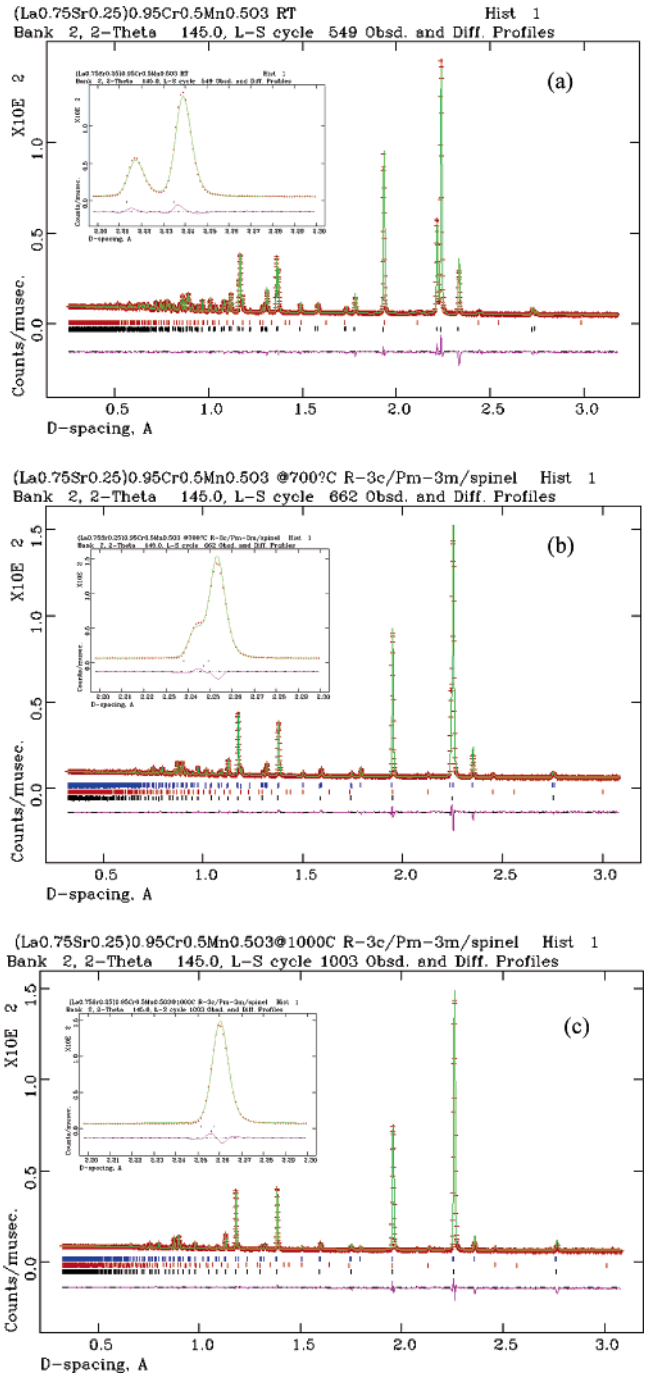

Figure 2. Neutron diffraction pattern of $La_{0.75}Sr_{0.25}Cr_{0.5}Mn_{0.5}O_3$ at room temperature (a), 700 °C (b), and 1000 °C (c). Tick marks, upper, spinel; down, $R\bar{3}c$ for (a); upper, $R\bar{3}c$; middle, spinel; down, $Pm\bar{3}m$ for (b) and (c). Inserts show the split of the main diffraction peaks at $d \sim 2.3$ Å.

absence of oxygen vacancies. As a consequence, the occupancies of La, Sr, and O were fixed as 0.75, 0.25, and 1 during the refinement. Thus, the correct formula should be

Table 2. Room-Temperature Structure Parameters of $La_{0.75}Sr_{0.25}Cr_{0.5}Mn_{0.5}O_3$ Prepared at 1400 °C Obtained from Neutron Powder Diffraction Data

atom	site	occupancy	x	y	z	U_{iso} (Å^2)
			Perovskite Phase[a]			
La	2a	0.75	0.25	0.25	0.25	0.0089(2)
Sr	2a	0.25	0.25	0.25	0.25	0.0089(2)
Cr	2b	0.5	0	0	0	0.0131
Mn	2b	0.5	0	0	0	0.0131
O	6e	1	−0.7947(1)	0.7053(1)	0.25	0.0104(1)
			Spinel Phase[b]			
Mn	8a	1	1/8	1/8	1/8	0.0131
Mn	16d	0.32(5)	1/2	1/2	1/2	0.0131
Cr	16d	0.68(5)	1/2	1/2	1/2	0.0131
O	32e	1	0.2642(1)	0.2642(1)	0.2642(1)	0.0299(2)

[a] Space group $R\bar{3}c$ (167); a = 5.4479(1) Å, α = 60.477(1)°, V = 115.563(1) Å^3, Z = 2. R_{wp} = 3.15%, R_p = 4.12%, χ_{red}^2 = 4.86. The second spinel phase is about 0.26%. [b] Space group $Fd\bar{3}m$ (227); a = 8.453(4) Å, V = 603.99(4) Å^3, Z = 8.

$La_{0.75}Sr_{0.25}Cr_{0.5}Mn_{0.5}O_3$ and therefore we use $La_{0.75}Sr_{0.25}Cr_{0.5}Mn_{0.5}O_{3-\delta}$ as the formula in the rest of this paper.

The $R\bar{3}c$(167) model fits most of the peaks in the neutron diffraction pattern; however, the two peaks at d = 2.115 and 2.443 Å cannot be fitted by this model (Figure 2a). Models of perovskite with lower symmetry do not fit these two peaks either. Although these diffraction peaks cannot be indexed by the three strongest lines of known La- or Sr-containing compounds, they are fairly close to the (311) and (400) diffractions of cubic Mn−Cr−O spinel phases such as $MnCr_2O_4$ (JCPDF 76-1614) and $Mn_{1.5}Cr_{1.5}O_4$ (JCDF 33-892), even though the minor Mn−Cr−O second phase was not observed by X-ray diffraction. This is entirely consistent with the observation that the perovskite was not A-site deficient, even though the overall composition was deficient of La/Sr. The intensity and number of peaks from the spinel phase with space group $Fd\bar{3}m$(227) does not change with temperature up to 1000 °C. The refined composition is $Mn(Mn_{2/3}Cr_{4/3})O_4$. The refined lattice parameter a = 8.453 Å from neutron diffraction is consistent with that reported for $Mn_{1.5}Cr_{1.5}O_4$ (8.455 Å) and differs from that of $MnCr_2O_4$ (8.437 Å). The refined fraction of the second Mn−Cr−O spinel phase is 0.26%. The fraction of the spinel phase was therefore fixed to 0.26% during the refinement of the high-temperature patterns. Details of the room-temperature neutron diffraction refinement are presented in Table 2.

3.2. Evolution of Phase and Structure with Temperature. The properties of materials are correlated with their structure. For $La_{0.75}Sr_{0.25}Cr_{0.5}Mn_{0.5}O_3$ the high-temperature conductivity and thermal expansion of $La_{0.75}Sr_{0.25}Cr_{0.5}Mn_{0.5}O_3$ have been examined and some changes with temperature observed.

A sample with a nominal composition of "$(La_{0.75}Sr_{0.25})_{0.95}Cr_{0.5}Mn_{0.5}O_3$" was pressed into a cylinder with a diameter of 13 mm and a length of about 100 mm. After the cylinder was fired at 1500 °C for 36 h, the diameter of the cylinder was about 12 mm. The as-prepared cylinder was used for a dilatometry test in air. As shown in Figure 3, the linear thermal expansion coefficient (TEC) of LSCM is 8.9 × 10^{-6} K^{-1} in the temperature range of 64−435 °C and 10.1 × 10^{-6} K^{-1} between 520 and 956 °C. There is a change in slope at 435−520 °C, which may relate to phase transformation behavior. The average TEC between 64 and 956 °C is 9.3

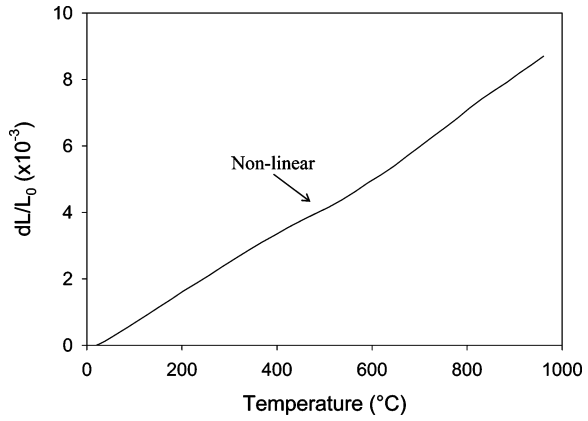

Figure 3. Thermal expansion of $La_{0.75}Sr_{0.25}Cr_{0.5}Mn_{0.5}O_3$ at high temperatures in air. The heating rate is 3 °C/min.

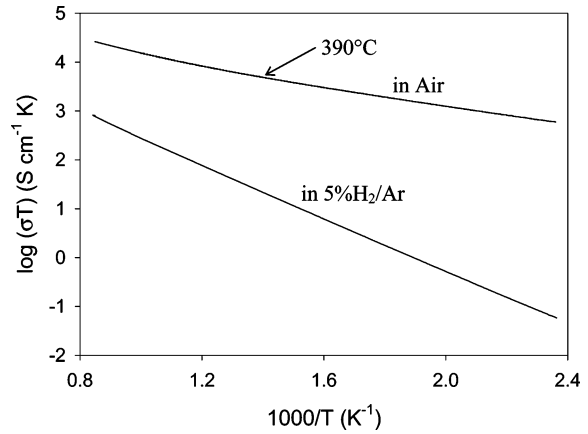

Figure 4. Total conductivity of $(La_{0.75}Sr_{0.25}Cr_{0.5})_{0.95}Mn_{0.5}O_{3-\delta}$ in air and 5 %H_2/Ar at different temperatures.

$\times$ 10^{-6} K^{-1}. This is close to the TEC value for yttria-stabilized zirconia, the most commonly used SOFC electrolyte (10.3×10^{-6} K^{-1}).[5]

The conductivities of LSCM in air and 5% H_2/Ar were also measured by the four-terminal dc method. In a previous study which used both ac impedance and dc techniques to separate bulk and grain boundary elements, the change in activation energy in both air and 5% H_2/Ar was reported as insignificant over the tested temperature range.[10] On more careful inspection of the data, it was found that there is a small activation energy change for the conductivity in air which could be related to a phase change. The extracted grain conduction activation energy in air is 0.19 $\pm$ 0.01 eV between 150 and 390 °C and 0.26 $\pm$ 0.02 eV between 390 and 903 °C. The activation energy in 5% H_2/Ar is 0.54 $\pm$ 0.01 eV between 150 and 905 °C. No changes in activation energies were observed over the temperature range in 5% H_2/Ar, suggesting that a phase change is unlikely when cooling in 5% H_2/Ar; however, the change in conductivity behavior in air (Figure 4) may relate to a possible phase change, which is consistent with the dilatometric test. To investigate these phenomena, an in situ high-temperature structural study has been performed.

The dependence of the conductivity upon oxygen partial pressure at 900 °C is shown in Figure 5. LSCM is a p-type conductor at low pO_2 and its conductivity drops with decreasing pO_2. The decrease of conductivity happens at a pO_2 of 10^{-10} atm at 900 °C due to the loss of oxygen.

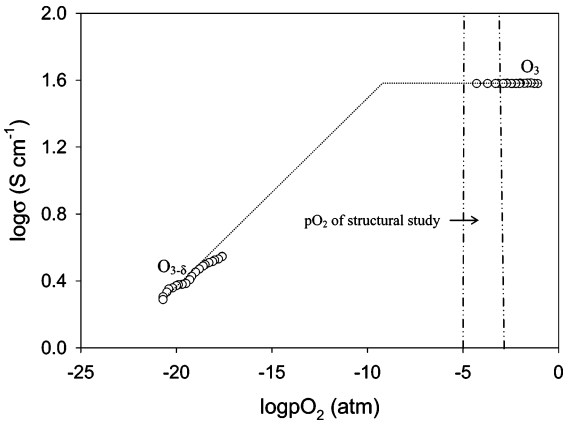

Figure 5. Isothermal conductivity vs pO_2 diagram for $La_{0.75}Sr_{0.25}Cr_{0.5}Mn_{0.5}O_{3-\delta}$ at 900 °C. Lines show extrapolated conductivity behavior illustrating onset of oxygen loss. The oxygen partial pressure range relevant to the neutron diffraction experiments is denoted.

Therefore, it is assumed that the oxygen content remains stoichiometric for a pO_2 higher than 10^{-10} atm. The vanadium sample holder might act as an oxygen getter at the highest temperatures; however, the sample and the interior of the can were not sealed from the vacuum and the can had previously been equilibrated in the vacuum, so it seems that the vanadium is unlikely to act as a getter here. This was further confirmed by the lack of visible change in the inside of the can after the experiments. During neutron diffraction, the sample was placed in a partially sealed vanadium container with a vacuum of $\sim 10^{-5}$ atm. Therefore, the pO_2 of the $La_{0.75}Sr_{0.25}Cr_{0.5}Mn_{0.5}O_3$ sample in the high-temperature neutron diffraction experiment is assumed to be in the range of 10^{-5} to 10^{-3} atm. Thus, any phase transition is unlikely to be due to the reducing vanadium sample holder because the same phenomena were observed when high-temperature X-ray diffraction was performed in air. Decomposition or significant loss of oxygen is thus unlikely under the experimental conditions.

To further confirm that no weight change occurs under vacuum, TGA analysis of the LSCM sample was carried out in Ar (which has a similar pO_2 to the vacuum) heating up to 900 °C and held isothermally for 2 h. No significant weight loss could be detected, giving an upper limit for any oxygen loss on heating of <0.04 wt %, i.e., <0.01 oxygen per perovskite unit. This is much smaller than that of 1.5 wt % when the LSCM sample was heated in 5% H_2/Ar at 900 °C.[10] The oxygen stoichiometry change on heating in vacuum is very small, or possibly nil, so it is unlikely to trigger a phase transition.

In the high-temperature neutron diffraction study, the data at 20, 200, 300, and 400 °C may be refined well with the rhombohedral perovskite model. When combined rhombohedral $R\bar{3}c$ and cubic $Pm\bar{3}m$ models are applied to the patterns at such temperatures, the refined fraction of the cubic phase tends to zero, indicating that the rhombohedral phase is dominant. The splitting of the main peaks gets less and less with increasing temperature as shown in Figure 2. At 1000 °C, the splitting of the main peak is insignificant, suggesting that the material exhibits a structure with higher symmetry. According to the group−subgroup relationships among the perovskite structures, the next possible higher

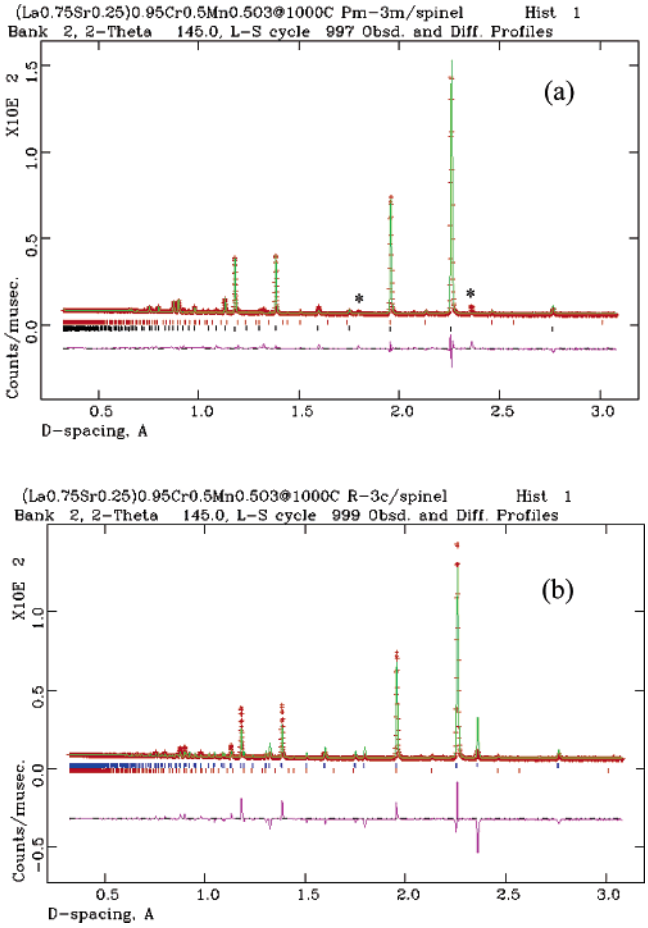

Figure 6. Neutron diffraction pattern of $La_{0.75}Sr_{0.25}Cr_{0.5}Mn_{0.5}O_3$ at 1000 °C fitted to $Pm\bar{3}m$ perovskite (lower tick marks) and spinel (upper tick marks). * = unindexed peaks from $R\bar{3}c$ phase (a) and $R\bar{3}c$ perovskite (upper tick marks) and spinel (lower tick marks) (b).

symmetry after $R\bar{3}c$ would be $Pm\bar{3}m$.[19] At 500 °C and above, the splitting of the main peak at $d = 2.25$ Å decreases, indicating less lattice distortion and the tendency to higher symmetry (Figure 2). The relative intensity of an important $R\bar{3}c$ peak absent from the cubic variant at $d = 2.33$ Å also decreased with temperature but had not disappeared by 1000 °C.

After a review of the pattern at 1000 °C, it was found that splitting of the main peak is insignificant; therefore, the cubic phase is dominant. However, some rhombohedral phase still remained at 1000 °C, as evidenced by the existence of the peak at $d = 2.33$ Å (Figure 6). Very poor fitting was observed when the rhombohedral $R\bar{3}c$ model was solely applied for the pattern at 1000 °C (Figure 6b), indicating that both cubic and rhombohedral phases coexist at 1000 °C. Good fitting was achieved when the combined $Pm\bar{3}m$/$R\bar{3}c$ model was used for the refinement. The refined fractions for the cubic phase and rhombohedral phases are 85.5% and 14.2%, respectively, at 1000 °C. The $R\bar{3}c \rightarrow Pm\bar{3}m$ transition was incomplete even at a temperature as high as 1000 °C.

At 600 °C, the presence of two phases is even more clearly demonstrated. Poor fitting with large *R*-values and goodness-to-fit was observed when the pattern was fitted with only one phase (Figure 7). Better fitting has been achieved with the combined $Pm\bar{3}m/R\bar{3}c$ model with R_{wp}, R_p, and χ^2 of 4.54%, 5.91%, and 7.014, respectively (Figure 7c), compared

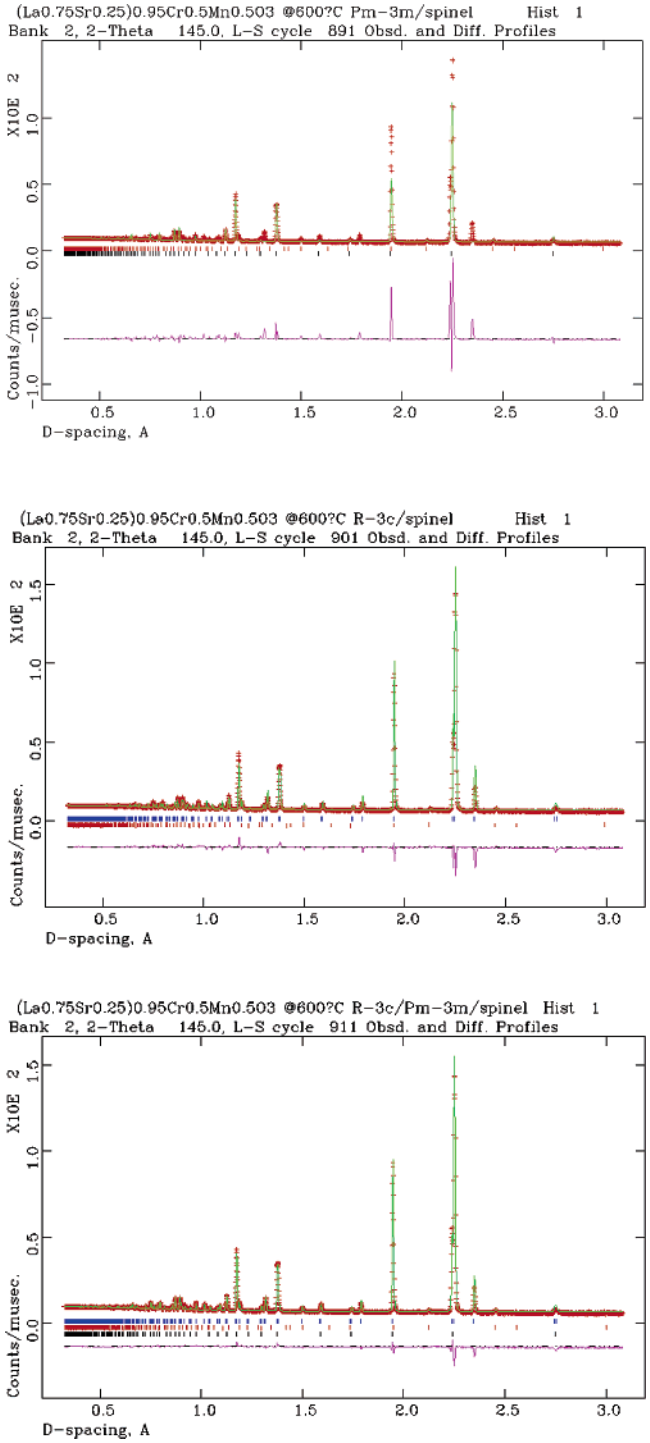

Figure 7. Neutron diffraction pattern of $La_{0.75}Sr_{0.25}Cr_{0.5}Mn_{0.5}O_3$ at 600 °C fitted with $Pm\bar{3}m$ (a) and $R\bar{3}c$ (b) models and combined $Pm\bar{3}m$ and $R\bar{3}c$ model (c), all with minor spinel impurity.

to single-phase models which gave *R*-values over 10 and χ^2 over 20. Therefore, the two-phase model, together with the minor spinel second phase, was used to fit the patterns between 500 and 1000 °C.

Table 3 lists the refined parameters of $La_{0.75}Sr_{0.25}Cr_{0.5}Mn_{0.5}O_3$ at selected temperatures. The A site is shared by La and Sr and the B-site by Cr and Mn. The neutron scattering lengths of Cr and Mn on the B-sites are 3.635 and −3.73 fm, respectively; thus, it is fairly precise to determine their occupancy by neutron diffraction for both $R\bar{3}c$ and $Pm\bar{3}m$ models. Also, due to the comparable amounts

Table 3. Refined Structure Parameters for $La_{0.75}Sr_{0.25}Cr_{0.5}Mn_{0.5}O_3$ between 200 and 1000 °C

		200 °C	400 °C	600 °C		800 °C		1000 °C	
atom	parameter	$R\bar{3}c$	$R\bar{3}c$	$R\bar{3}c$	$Pm\bar{3}m$	$R\bar{3}c$	$Pm\bar{3}m$	$R\bar{3}c$	$Pm\bar{3}m$
La/Sr	x	1/4	1/4	1/4	0	1/4	0	1/4	0
	y	1/4	1/4	1/4	0	1/4	0	1/4	0
	z	1/4	1/4	1/4	0	1/4	0	1/4	0
	U_{iso} (Å^2)	0.0092(1)	0.0073(1)	0.0125(2)	0.0125(2)	0.0161(3)	0.0161(3)	0.0167(2)	0.0167(2)
occupancy	La	0.75	0.75	0.75	0.75	0.75	0.75	0.75	0.75
	Sr	0.25	0.25	0.25	0.25	0.25	0.25	0.25	0.25
Cr/Mn	x	0	0	0	1/2	0	1/2	0	1/2
	y	0	0	0	1/2	0	1/2	0	1/2
	z	0	0	0	1/2	0	1/2	0	1/2
	U_{iso} (Å^2)	0.0131	0.0131	0.0131	0.0131	0.0131	0.0131	0.0131	0.0131
occupancy	Cr	0.513(3)	0.528(3)	0.530(9)	0.497(2)	0.518(1)	0.512 (1)	0.514(3)	0.515(1)
	Mn	0.487(3)	0.472(3)	0.470(9)	0.503(2)	0.482(1)	0.488(1)	0.486(3)	0.485(1)
O	x	−0.2072(1)	−0.2092(1)	−0.2033(2)	0	−0.1964(4)	0	−0.1947(9)	0
	y	0.7072(1)	0.7092(1)	0.7033(2)	1/2	0.6964(4)	1/2	0.6947(9)	1/2
	z	1/4	1/4	1/4	1/2	1/4	1/2	1/4	1/2
	U_{iso} (Å^2)	0.0120(1)	0.0125(1)	0.0162(2)	0.0163(2)	0.0230(3)	0.0229(3)	0.0307(3)	0.0307(3)
occupancy	O	1.0	1.0	1.0	1.0	1.0	1.0	1.0	1.0
R_{wp} (%)		5.01	5.45	4.54		6.07		3.14	
R_p (%)		7.47	8.68	5.91		7.64		4.48	
χ_{red}^2		5.905	7.883	7.01		9.285		5.837	

of Cr and Mn on the B site and the opposite signs for the scattering lengths, the net scattering length for the Cr/Mn site is very weak, and the error in determination of the corresponding thermal factors is huge.[28] The refinement is very unstable if the thermal factors of Cr and Mn in either phase are refined. Therefore, the thermal factor of Cr/Mn from X-ray diffraction was applied to the neutron refinement. It was found that the occupancies of Cr and Mn are fairly close to the starting composition of 50% each in both rhombohedral and cubic phases, indicating that no phase segregation occurs between phases. As expected, the thermal factors of La/Sr and O increase with increasing temperature.

The fraction of each phase may be refined as shown in Figure 8. It was found that the fraction of the cubic phase increased with temperature and, accordingly, the fraction of the rhombohedral phase decreased. At 1000 °C, the fraction of the cubic phase reached 85.5% but still the $R\bar{3}c \rightarrow Pm\bar{3}m$ phase change was incomplete. This transition should be complete around 1100 °C by extrapolating the data points from Figure 8. The observed almost linear relationship between temperature and the cubic phase fraction indicates that, most likely, thermodynamic equilibrium was achieved for the phase transition since it is unlikely to be linear if it is under kinetic control. This was confirmed by performing in situ XRD studies at 800 °C over a period of 5 h with no change in peak positions or intensities.

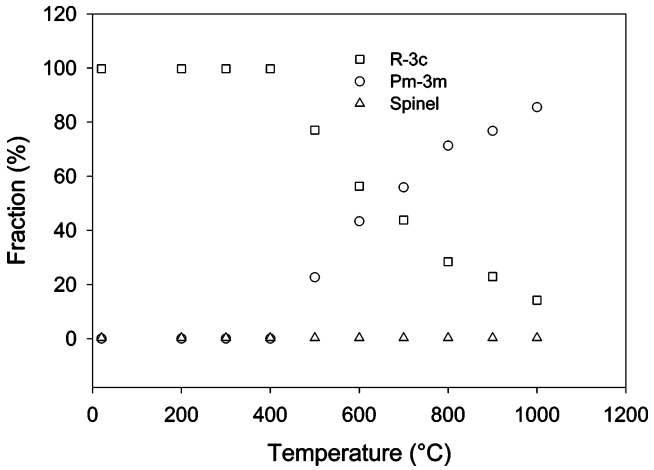

Figure 8. Fraction of different phases in the perovskite oxide $La_{0.75}Sr_{0.25}Cr_{0.5}Mn_{0.5}O_3$ at different temperatures.

Figures 9 and 10 show the lattice parameters and cell volume of each phase plotted against temperature. The linear increase with temperature confirms that the unit cells for Rietveld refinement were correctly chosen. The beta angle of the rhombohedral phase decreased from 60.5 to 60.1° between 20 and 1000 °C. This indicates the rhombohedral distortion of the lattice becomes less as the symmetry approaches cubic. The linear volume change of the rhombohedral and cubic phase fractions against temperature indicates that the phase transition is second order, which is also allowed by the group−subgroup relationship analysis.[19]

Figure 11 shows the normalized primitive perovskite lattice volume of the $R\bar{3}c$ and $Pm\bar{3}m$ phases against temperature. The primitive cell volume of the cubic phase is slightly larger than that of the rhombohedral phase at the same temperature. The $R\bar{3}c \rightarrow Pm\bar{3}m$ phase transition is not unusual in perovskite oxides. It was reported that perovskite oxide $Pr_{1-x}Sr_xMnO_3$ exhibits this phase transition at high temperature.[29] The perovskite-related α-AlF_3 also undergoes the same phase transition at 470 °C.[30] Most phase transitions in perovskite oxides happen in a narrow temperature range. There are few reports of a significant two-phase coexistence area in perovskite oxides. The $P2_1/n$ and $R\bar{3}$ phases coexist over 685−775 K in $SrLaCuRuO_6$ and from 610 to 730 K in $SrLaNiRuO_6$.[31] The $I4/mcm$ and $Ibmm$ phases also coexist in $Pr_{1-x}Sr_xMnO_3$ with the reported temperature range of the two-phase area being <100 °C.[29] The $R\bar{3}c \rightarrow Pm\bar{3}m$ phase transition is straightforward in the $Pr_{1-x}Sr_xMnO_3$ high-temperature phase diagram and no two-phase area was

(28) Alonso, J. A.; Martinez-Lope, M. J.; Casais, M. T.; Martinez, J. L.; Pomjakushin V. *Eur. J. Inorg. Chem.* **2003**, *15*, 2839.
(29) Knizek, K.; Hejtmanek, J.; Jirak, Z.; Martin, C.; Hervieu, M.; Raveau, B.; Andre, G.; Bouree, F. *Chem. Mater.* **2004**, *16*, 1104.
(30) Chupas, P. J.; Chaudhuri, S.; Hanson, J. C.; Qiu, X. Y.; Lee, P. L.; Shastri, S. D.; Billinge, S. J. L.; Grey, C. P. *J. Am. Chem. Soc.* **2004**, *126*, 4756.
(31) Gateshki, M.; Igartua, J. M. *Mater. Res. Bull.* **2003**, *38*, 1893.

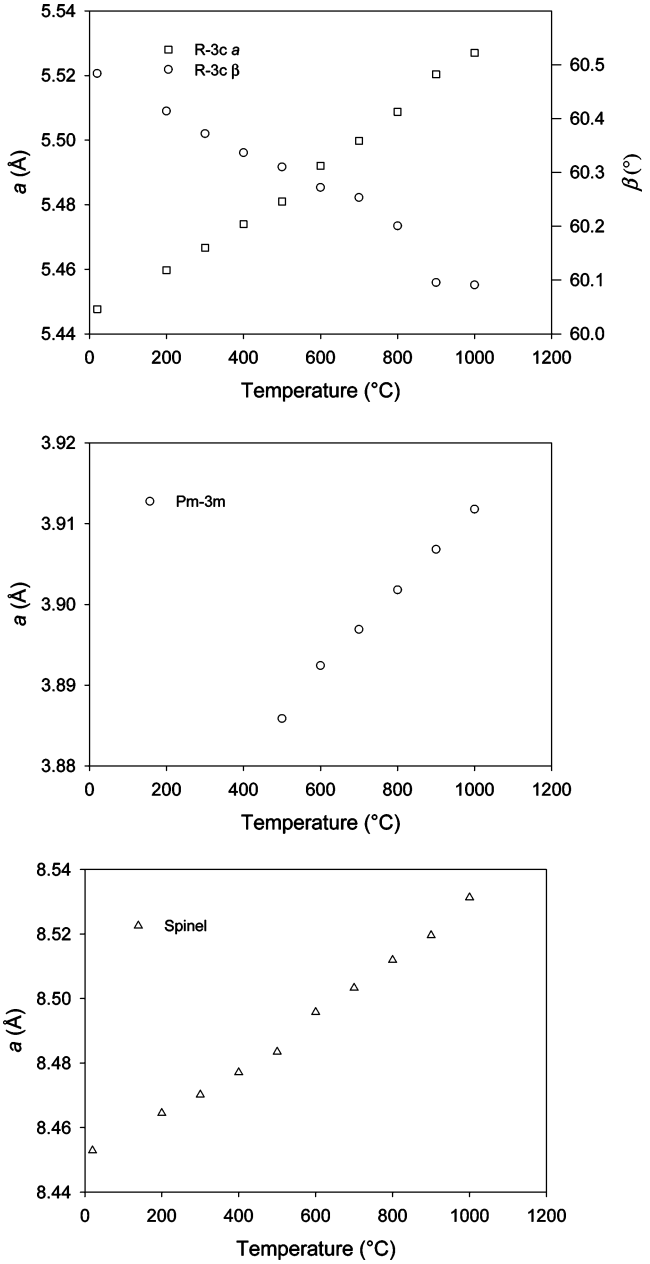

Figure 9. Variation of the lattice parameters of different phases in $La_{0.75}Sr_{0.25}Cr_{0.5}Mn_{0.5}O_3$ as a function of temperature; error values are within symbols.

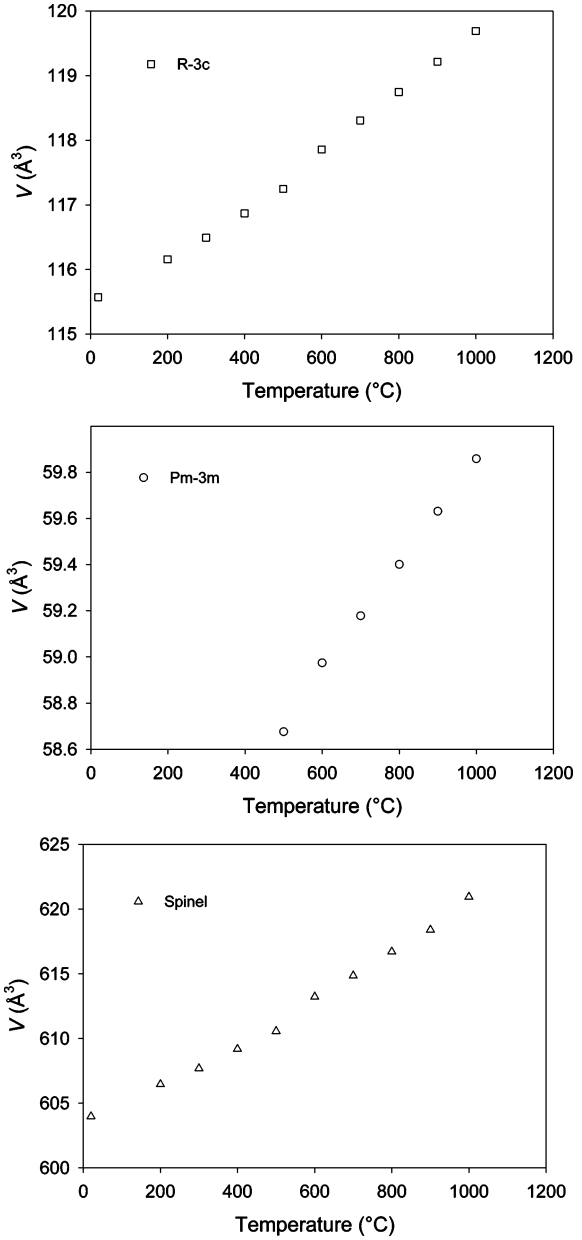

Figure 10. Variation of the cell volume of different phases in $La_{0.75}Sr_{0.25}Cr_{0.5}Mn_{0.5}O_{3-\delta}$ as a function of temperature; error values are within symbols.

detected at the $R\bar{3}c/Pm\bar{3}m$ border. In contrast, in our experiments, these phases coexist in $La_{0.75}Sr_{0.25}Cr_{0.5}Mn_{0.5}O_3$ over a wide temperature range from 500 to over 1000 °C. The phase transition should be completed by around 1100 °C according to extrapolation of the data in Figure 8. The total two-phase coexistence range would be roughly 600 °C, which is much larger than the reported other phase systems.

The possibility that a change of the oxygen stoichiometry in $La_{0.75}Sr_{0.25}Cr_{0.5}Mn_{0.5}O_3$ on heating caused the phase segregation can be discounted because it was found that LSCM retained the rhombohedral structure after heating the sample under vacuum ($pO_2 \approx 10^{-5}$ atm) at 1000 °C for 10 h and cooling down under vacuum and as mentioned above no change in oxygen content was detectable under conditions similar to those of the neutron diffraction experiment. There is also no evidence of any cation redistribution leading to the phase segregation; thus, the driving force for the two-phase region must be thermodynamic with the two poly-

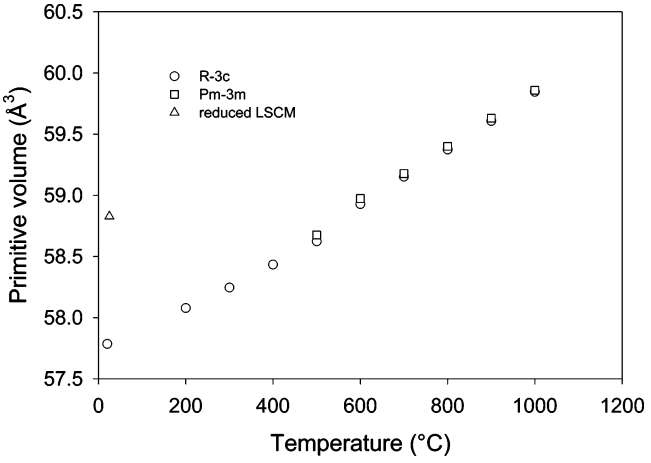

Figure 11. Normalized volume against temperature for the different phases; error values are within symbols.

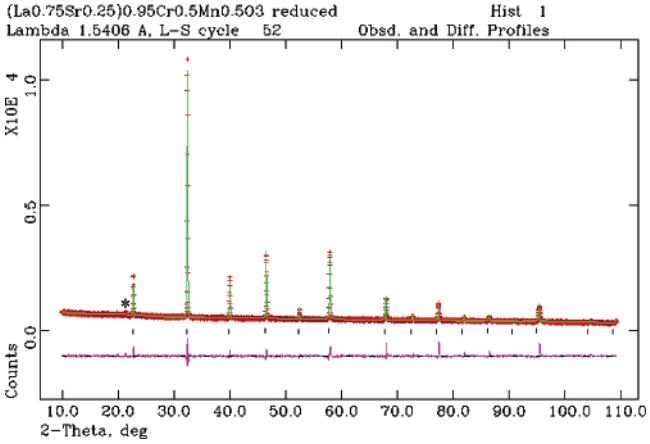

Figure 12. X-ray diffraction pattern of $La_{0.75}Sr_{0.25}Cr_{0.5}Mn_{0.5}O_{3-\delta}$ prepared at 1400 °C and reduced in 5 %H_2/Ar at 900 °C for 120 h. * Vaseline.

Table 4. Structure Parameters of $La_{0.75}Sr_{0.25}Cr_{0.5}Mn_{0.5}O_3$ Prepared at 1400 °C and after Reduction at 900 °C/120 h in 5% H_2/Ar Obtained from X-ray Diffraction Data[a]

atom	site	occupancy	x	y	z	U_{iso} (Å^2)
La	1a	0.75	0	0	0	0.0184(6)
Sr	1a	0.25	0	0	0	0.0184(6)
Cr	1b	0.5	0.5	0.5	0.5	0.0166(10)
Mn	1b	0.5	0.5	0.5	0.5	0.0166(10)
O	3e	0.924(23)	0	0.5	0.5	0.035(5)

[a] Space group $Pm\bar{3}m$ (221); $a = 3.8942(1)$ Å, $V = 59.06(1)$ Å^3, $Z = 1$. $R_{wp} = 6.67\%$, $R_p = 4.33\%$, $\chi_{red}^2 = 2.293$.

morphs in equilibrium rather than some form of chemical segregation.

The second-order phase transition of LSCM on heating is beneficial for SOFC fabrication because delamination of the electrolyte/anode interface due to a sudden phase transition leading to abrupt volume change can be avoided. Since the dominant phase of LSCM in air at high temperature is the cubic one, when reduced at 900 °C, the resultant phase is also cubic which may minimize redox stresses.

3.3. Structure of Reduced $La_{0.75}Sr_{0.25}Cr_{0.5}Mn_{0.5}O_{3-\delta}$. The XRD pattern of a sample of $La_{0.75}Sr_{0.25}Cr_{0.5}Mn_{0.5}O_{3-\delta}$ that had been reduced at 900 °C in 5% H_2/Ar for 120 h is shown in Figure 12. No second phase was detected. Good fitting and a lower R-value were achieved when the cubic $Pm\bar{3}m$ model was applied. The refined structure details are listed in Table 4. Figure 13 shows the neutron diffraction pattern of reduced $La_{0.75}Sr_{0.25}Cr_{0.5}Mn_{0.5}O_{3-\delta}$ at room temperature. The fraction of main phase is 99.5% with space group $Pm\bar{3}m$. The remaining 0.5% seems to be MnO that arises from the reduced spinel in accord with the MnO−Cr_2O_3 phase diagram,[32] although the expected trace amount of cubic Cr-rich spinel was not detected. With the segregation of MnO from the spinel phase decreasing the amount of spinel remaining and some overlap with the rock salt MnO, which has a similar oxygen lattice, the neutron diffraction signal would be too weak to be easily detected. The refined oxygen occupancy of the reduced $La_{0.75}Sr_{0.25}Cr_{0.5}Mn_{0.5}O_{3-\delta}$ is 0.92(2) and 0.95(2), respectively, from XRD and neutron

(32) Jung, I.-H. *Solid State Ionics* **2006**, *177*, 765.

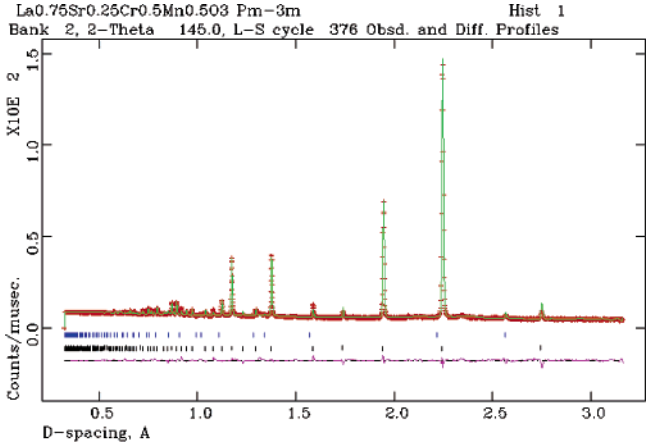

Figure 13. Room-temperature neutron diffraction pattern of reduced $La_{0.75}Sr_{0.25}Cr_{0.5}Mn_{0.5}O_{3-\delta}$ prepared at 1400 °C, then further reduced at 900 °C for 120 h, and cooled down in 5 %H_2/Ar. Tick marks, upper, MnO; down, $Pm\bar{3}m$.

Table 5. Structure Parameters of $La_{0.75}Sr_{0.25}Cr_{0.5}Mn_{0.5}O_3$ Prepared at 1400 °C and after Reduction at 900 °C/120 h in 5% H_2/Ar Obtained from Neutron Diffraction Data[a]

atom	site	occupancy	x	y	z	U_{iso} (Å^2)
La	1a	0.75	0	0	0	0.0116(3)
Sr	1a	0.25	0	0	0	0.0116(3)
Cr	1b	0.5	0.5	0.5	0.5	0.0166
Mn	1b	0.5	0.5	0.5	0.5	0.0166
O	3e	0.95(2)	0	0.5	0.5	0.0456(4)

[a] Space group $Pm\bar{3}m$ (221); $a = 3.8892(1)$ Å, $V = 58.828(1)$ Å^3, $Z = 1$. $R_{wp} = 4.75\%$, $R_p = 3.87\%$, $\chi_{red}^2 = 1.811$.

diffraction indicating existence of oxygen vacancies in reduced sample and a δ value of 0.15, assuming neutron diffraction to provide a more reliable measure (Table 5). According to both XRD and neutron diffraction, the volume of the reduced phase is about 1.7% larger than the oxidized form at room temperature. This is consistent with that previously reported,[10] which was derived under slightly more reducing conditions.

Conclusions

The actual composition of the nominal A-site deficient perovskite $(La_{0.75}Sr_{0.25})_{0.95}Cr0.5Mn_{0.5}O_3$ is in fact close to A-site stoichoimetric according to neutron diffraction. The work presented here clearly shows that the perovskite oxide $La_{0.75}Sr_{0.25}Cr_{0.5}Mn_{0.5}O_{3-\delta}$ (LSCM) undergoes a $R\bar{3}c \rightarrow Pm\bar{3}m$ rhombohedral to cubic phase transition from 500 to over 1000 °C. The two-phase coexistence spans a temperature range of about 600 °C, which is much wider than previously reported for other perovskite oxides, ~100 °C. The dominant phase of LSCM in air has the same symmetry as the reduced variant at high temperature, which may alleviate redox shock on fuel cell cycling.

Acknowledgment. We thank EPSRC (Platform grant) and the European Union RealSOFC Project for funding. We also thank Dr. Ron Smith at ISIS, Rutherford, in assistance with data collection. One of the authors (Tao) is grateful to EaStCHEM for a fellowship.

CM061413N